



## Research Article

Ferroic glass behavior in (Bi,Na)TiO<sub>3</sub>-based lead-free electroceramics

Julio Cesar Camilo Alborno Diaz<sup>a,b</sup>, Michel Venet<sup>a</sup>, Ariano De Giovanni Rodrigues<sup>a</sup>,  
David Antonio Barbosa Quiroga<sup>a</sup>, Francesco Cordero<sup>c</sup>, Paulo Sergio da Silva Jr.<sup>a,\*</sup>

<sup>a</sup> Department of Physics, Federal University of São Carlos, Brazil

<sup>b</sup> Center of Science and Technology of Materials, Energy and Nuclear Research Institute, São Paulo, SP, Brazil

<sup>c</sup> CNR-ISM, Istituto di Struttura della Materia, Area della Ricerca di Roma-Tor Vergata, Roma, Italy



## ARTICLE INFO

## Article history:

Received 13 April 2022

Received in revised form 25 May 2022

Accepted 30 May 2022

Available online 2 June 2022

## Keywords:

Ferroic glass

Lead-free ceramics

BNT

Relaxor

Tilt strain glass

Anelasticity

## ABSTRACT

Ferroic glass materials, that is, relaxors, spin glasses, and strain glasses attract special attention because of their intriguing physical properties and potential for novel technological applications. Here, several characterization techniques are used to demonstrate the occurrence of simultaneous relaxor and strain glass states in the ternary lead-free  $x\text{Bi}_{0.5}\text{Na}_{0.5}\text{TiO}_3\text{-yBi}_{0.5}\text{K}_{0.5}\text{TiO}_3\text{-zBaTiO}_3$  (BNBK) system. Hysteresis and current density loops measurements at different temperatures for a BNBK ceramic showed typical characteristics observed in BNT based ceramics containing the tetragonal  $P4bm$  phase. Above 400 K, slim loops like those of ferroelectric relaxors are observed. A phase transition with simultaneous relaxor and strain glass character is revealed by the dielectric and anelastic characterizations, which opens up a wide spectrum of possible applications. The minimum of elastic modulus shifts to higher temperatures as the frequency increases, obeying the Vogel-Fulcher relation, which clearly shows the occurrence of a strain glass state in this material. Similar characteristics are observed in the imaginary part of the dielectric permittivity, which demonstrates the relaxor character of this phase transition. The origin of this phenomenon was elucidated with the help of structural characterizations, such as Raman spectroscopy and high-resolution synchrotron X-ray diffraction, at different temperatures. This work provides an in-depth understanding of the structural changes that determine the phenomenology behind the observed ferroic glass behavior and the ferroelectric, dielectric, and mechanical properties of this ternary ceramic composition.

© 2022 Elsevier B.V. All rights reserved.

## 1. Introduction

Ferroic materials are relevant due to their strong potential for technological applications, such as sensors, actuators, transducers, memories, energy harvesting/storage, spintronics, and other multifunctional devices [1–3]. Ferroic orders, that is, ferroelectricity, ferromagnetism, ferroelasticity, and ferrotoroidicity, are characterized by physical properties that can be switched between two or more states through external stimuli, such as electric and magnetic fields or stress [1,4–6]. The coexistence between two or more of these orders can enable the emergence of new physical properties [1,7,8]. In general, the ferroic states arise from a disorder-order ferroic phase transition at a critical temperature ( $T_c$ ) and they have a long-range ordering of electric dipoles in ferroelectrics, for instance, or lattice strains in ferroelastics below  $T_c$  [1]. Nevertheless, some ferroic systems can undergo the break of the long-range ordering below  $T_c$ ,

with the consequent stabilization of a glassy non-ergodic state. These phenomena have been independently observed for ferroelectrics [9], ferromagnetics [10], and more recently for ferroelastic materials [11], and named relaxor, spin glass, and strain glass, respectively.

Ren et al. [12] proposed the concept of ferroic glass to unify glass phenomena in these ferroic systems. The ferroic glass state originates from a gradual freezing process of the disordered ferroic state, resulting in the so-called ferroic glass transition, which has unique features absent in a typical ferroic transition [12,13]. For instance, the strain glass behavior of materials can be identified by a peculiar thermal and frequency evolution of the mechanical response around the phase-transition region, measured from their anelastic properties. This mechanical phenomenon has been reported mainly for metallic systems, like Ti-Ni-based [14] and Ti-Pd-based shape-memory alloys [15], magnetic shape memory alloys [16], and recently, also in a few ceramics systems [17–19].

The origin of ferroic glass orders is still an open issue in most materials, so it has attracted the special attention of the scientific community. To top it off, materials with ferroic glass orders have

\* Corresponding author.

E-mail address: [psergio@ufscar.br](mailto:psergio@ufscar.br) (P.S. da Silva Jr).

exceptional potential for novel technological applications. Ferroelectric relaxors, for instance, have high dielectric permittivity in a wide temperature range due to their diffuse phase transition, which is extremely desirable for ceramic capacitor applications [2]. Also, the Invar and Elinvar effects observed in strain glasses of Ti-based alloys [20] make these materials relevant for many precision device applications [21].

In the last two decades, lead-free electroceramics have received considerable attention, and stand out those based on  $\text{Bi}_{0.5}\text{Na}_{0.5}\text{TiO}_3$  (BNT) materials [22–28]. BNT is an important base composition for various important solid solutions [22,23], such as, the binary  $x\text{Bi}_{0.5}\text{Na}_{0.5}\text{TiO}_3-y\text{BaTiO}_3$  (BNT-BT) and the ternary  $x\text{Bi}_{0.5}\text{Na}_{0.5}\text{TiO}_3-y\text{Bi}_{0.5}\text{K}_{0.5}\text{TiO}_3-z\text{BaTiO}_3$  (BNT-BKT-BT or BNBK) systems. The BNT-BT solid solution has been extensively studied because of its technological potential, mainly for compositions around the morphotropic phase boundary (MPB) between rhombohedral and tetragonal symmetries [29–31] where high piezoelectric coefficients and relatively high Curie temperatures can be obtained. On the other hand, the ternary BNBK system has been less studied despite its possible technological applications and the interesting phenomenology behind a more complex system. According to Yao and coauthors [18,32], BNT-BT materials show a typical ferroelastic phase transition for BT amounts less than 5 %, while for amounts between 5 % and 8 % they develop a strain glass transition. In addition, relaxor characteristics have been also reported for several BNT-BT ferroelectric compositions [33,34], however, despite ferroic glass states manifest mainly in disordered systems, the possible presence of these states (relaxor and/or strain glass) in ternary BNBK compositions has not been still investigated.

In this work, the possible emergence of a ferroic glass state in a BNBK ceramic, and its physical origin, were studied through the analysis of the ferroelectric hysteresis, dielectric, anelastic, vibrational and structural properties as a function of temperature.

## 2. Materials and methods

The BNBK ceramic composition was obtained following the nominal formula:



and labeled as BNBK82. This composition is located, at room temperature, within the tetragonal region of the ternary phase diagram of BNBK [31]. The target material was synthesized by solid-state reaction using high-purity  $\text{Bi}_2\text{O}_3$  (Acros Organics, > 99.9 %),  $\text{Na}_2\text{CO}_3$  (Acros Organics, > 99.8 %),  $\text{K}_2\text{CO}_3$  (Acros Organics, > 99 %),  $\text{BaCO}_3$  (Alfa Aesar, > 99.8 %) and  $\text{TiO}_2$  (Sigma-Aldrich, > 99.8 %) as precursors, which were weighted according to the nominal composition, and then mixed in a ball mill for 24 h. The mixture was calcined at 1123 K for 3 h, and ball milled again for 24 h to reduce particle sizes. Later the powder was uniaxially pressed, at 150 MPa, into cylindrical or plate-like thick samples, followed by isostatic pressing at 220 MPa. Finally, the resulting pellets were conventionally sintered at 1423 K for 3 h and dense ceramics with a relative density of 95.5 % were obtained. Apparent density was measured by the Archimedes method, using a precision balance (AUW220D, Shimadzu) and distilled water as medium. The ceramic samples were cut in geometries and sizes suitable to the different characterizations and then annealed at 900 K for 1 h. For electrical characterizations, platinum electrodes were sputtered on both major surfaces of the disk- or plate-like shaped samples.

“In situ” high-resolution synchrotron X-ray diffraction (XRD) measurements were performed in a  $\theta$ - $2\theta$  setup at the XRD2 beamline at the Brazilian Synchrotron Light Laboratory (CNPEM/LNLS), using an energy of 8 keV, from room temperature (298 K) up to 773 K.

Raman spectroscopy measurements were performed using a Raman spectrometer (T64000, Jobin Yvon) with resolution of  $1\text{ cm}^{-1}$  for temperatures between room temperature and 700 K. The line of 514.5 nm of an  $\text{Ar}^+$  laser was used as excitation source. The Raman spectra evolution between  $30\text{ cm}^{-1}$  and  $730\text{ cm}^{-1}$  was analyzed by considering the Raman peaks as Lorentzian functions, related to active Raman modes theoretically predicted for the crystalline structure [35].

Dielectric permittivity was measured from 298 to 875 K using an IET 7600 Plus high-precision LCR meter, over the 100 Hz to 1 MHz frequency range, with an applied ac voltage of 50 mV.

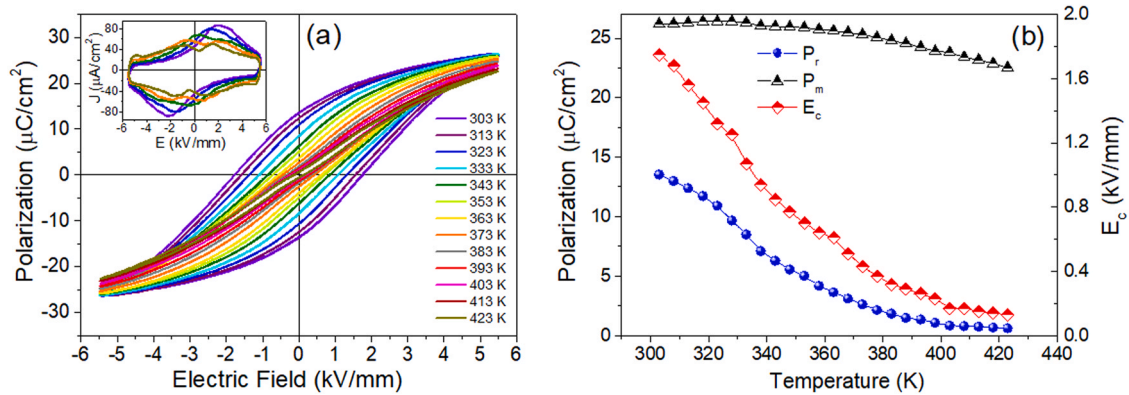
Ferroelectric hysteresis and current density loops were measured, at 100 Hz, using a Sawyer-Tower circuit, in a silicone oil bath, from 303 up to 423 K. For this measurement was used a triangular waveform provided by a function generator (33210A, Keysight) connected to a high voltage power supply (615-10-H-CE, Trek).

The complex Young's modulus ( $M^* = M' + iM''$ ) was measured using two different experimental setups: for frequencies between 0.5 Hz and 20 Hz – a *Dynamic Mechanical Analyzer* (DMA), PerkinElmer model DMA8000, in a three-point bending geometry was used. These measurements were performed from 298 to 870 K, with heating and cooling rates of 1 K/min, in air; and at 1 kHz – a *Flexural Vibration* setup, as described in Ref. [36]. In this case, the sample is suspended on two thin thermocouple wires and flexural resonance is electrostatically excited from 298 up to 850 K, in high-vacuum. Silver paint was applied to the sample in correspondence with the exciting/measuring electrode and to short the thermocouple. The mechanical spectra are displayed in terms of the real part of the complex Young's modulus ( $M'$ ) and the elastic energy loss coefficient  $Q^{-1} = M''/M'$ , so-called internal friction.

## 3. Results and discussion

Fig. 1a shows the ferroelectric hysteresis loops for a BNBK82 ceramic measured at several temperatures. At 303 K, the ferroelectric hysteresis loop has the typical behavior of a normal ferroelectric with remanent polarization ( $P_r$ ) and coercive field ( $E_c$ ) values of about  $14\text{ }\mu\text{C}/\text{cm}^2$  and 1.8 kV/mm, respectively. On the other extreme of temperature, 423 K, a slim and pinched loop can be observed. In BNT-based materials, the occurrence of pinched hysteresis loops is common for compositions containing a tetragonal  $P4bm$  phase [37–39]. This is a weakly polar phase with  $A$  and  $B$ -site cations displacements in opposite directions along the  $c$ -axis, and an unusual combination of in-phase  $a^0a^0c^+$  oxygen octahedra tilts, which can result in the antiparallel ordering of dipole moments [40,41]. Also, the weakly polar  $P4bm$  phase can easily transform into a long-range polar one (tetragonal  $P4mm$  or rhombohedral  $R3c$ ) under high electric fields, and in this case, pinched hysteresis loops are observed [38,42].

Inset of Fig. 1a shows the current density loops at different temperatures. The density current peak associated with the switching of polarization splits into two peaks between 323 and 343 K, which indicates the presence of the  $P4bm$  phase in this temperature range. The temperature evolution of the maximum polarization ( $P_m$ ),  $P_r$ , and  $E_c$  can be observed in Fig. 1b. Note that while  $P_r$  decreases  $\sim 13\text{ }\mu\text{C}/\text{cm}^2$  in the whole temperature range,  $P_m$  undergoes a slight decrease of only  $3.5\text{ }\mu\text{C}/\text{cm}^2$ , which reinforces the thesis that the  $P4bm$  phase exists and transforms into a long-range polar phase when electric field is applied. Furthermore,  $P_m$  starts to decrease between 333 and 343 K, which is the same temperature range where an inflection point in the  $P_r$  and  $E_c$  curves can be observed, and also, where peak splitting occurs in the current density loops. These anomalies may be related to the starting of a phase transition. Finally, when temperature is increased from  $\sim 400\text{ K}$ ,  $P_r$  and  $E_c$  remain almost constant with small values of  $0.5\text{ }\mu\text{C}/\text{cm}^2$  and 0.1 kV/mm, respectively, which results in typical slim loops (see



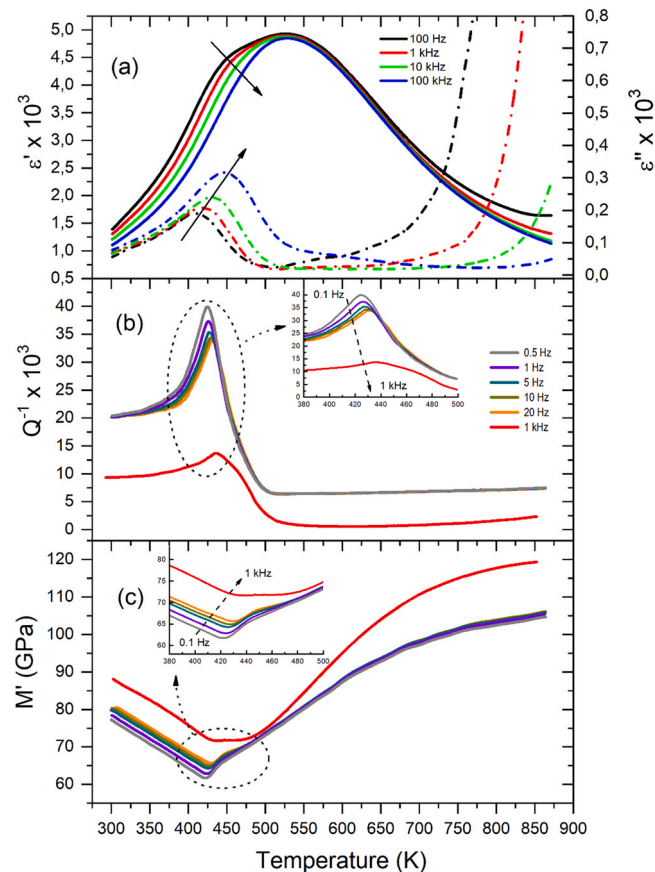
**Fig. 1.** (a) Ferroelectric hysteresis loops measured at several temperatures and (b) temperature dependence of the maximum polarization ( $P_m$ ), remanent polarization ( $P_r$ ), and coercive field ( $E_c$ ) for a BNBK82 ceramic. The inset in (a) represents the current density loops measured at different temperatures.

Fig. 1a) like those of ferroelectric relaxors. The occurrence of polar nano-regions (PNRs) in BNT-based materials with  $P4bm$  and/or  $R3c$  symmetry has been reported by several authors [34,43–48]. It is well-known that the A sites of the perovskite BNBK structure are randomly occupied by different ions ( $\text{Bi}^{3+}$ ,  $\text{Na}^+$ ,  $\text{Ba}^{2+}$  and  $\text{K}^+$ ), which causes the polar clusters to be locally different in shape and composition and, consequently, their temperature evolution is also different [49,50]. This is the origin of the relaxor behavior in most of the ferroelectric materials [51]. Despite that, at room temperature, the hysteresis loop evidences a long-range polar ordering, which is a characteristic of the average structure with  $P4mm$  symmetry, already reported for this material [31]. In this way, one can think of a possible scenario where the fraction of the  $P4mm$  polar phase decreases when temperature is raised, with the corresponding increase of any non-polar phase. Thus, at about 400 K the phase fraction of  $P4mm$  may be zero or small enough to lose long-range ordering, and the remaining PNRs of the weakly polar  $P4bm$  phase are embedded in a non-polar matrix.

Relaxor ferroelectrics have a peculiar dielectric response with high permittivity over a wide temperature range and strong frequency dispersion. Fig. 2a shows the temperature dependence of the real ( $\epsilon'$ ) and imaginary ( $\epsilon''$ ) parts of the complex dielectric permittivity at different frequencies for a BNBK82 ceramic. In fact, between 410 and 450 K, the  $\epsilon''$  curves show a strong frequency-dependent peak, like a typical relaxor ferroelectric. In correspondence with these peaks in  $\epsilon''$ , a frequency-dependent anomaly (shoulder) in the  $\epsilon'$  curves can be also observed. This anomaly appears to be a frequency-dependent peak superposed with a broad frequency-independent dielectric peak at about 530 K ( $T_m$ ). The imaginary dielectric constant is not sensitive to the peak at  $T_m$ , except for the exponential increase starting around  $T_m$ , at 100 Hz, which characterizes the increase in DC conductivity.

The shoulder below  $T_m$  has been related to a threshold between different dielectric relaxation processes [38,52]. Recently, Fan et al. [34] identified the temperature where the shoulder is observed ( $T_s$ ) is directly impacted by rapid cooling, biased cooling, and compressed cooling treatments while  $T_m$  is unaffected by these treatments in BNT-based ceramics. They suggested that internal stress gradients originating from defect accumulation are responsible for the size of PNRs and play a critical role in the dielectric relaxation of these materials at  $T_s$ .

On the other hand, the frequency-independent dielectric peak at  $T_m$  has been associated with a diffuse phase transition by several authors [43,53–56]. Nevertheless, recently Diaz et al. [57] demonstrated the origin of this peak in BNT ceramics is the presence of interfacial polarization involving space-charge defects related to oxygen vacancies that develop in the grain and grain boundaries and, therefore, no phase transition occurs at  $T_m$ . Thus, it can be thought



**Fig. 2.** Temperature dependence of the dielectric and mechanical responses, at different frequencies, for a BNBK82 ceramic. (a) Real  $\epsilon'$  and imaginary  $\epsilon''$  parts of dielectric permittivity, (b) Internal friction  $Q^{-1}$  and (c) Young's modulus  $M'$ . Insets in the  $Q^{-1}$  and  $M'$  graphs show a magnification of the temperature region where the anomalies were observed.

that the diffuse phase transition with a typical relaxor characteristic occurs around  $T_s$  for the BNBK82 ceramic.

Internal stress gradients can be related to the dielectric relaxation in the BNBK82 ceramic as proposed for some BNT based materials [57]. In this way, internal friction  $Q^{-1}$  and Young's modulus  $M'$  measurements were performed to verify the relationship between the dielectric and mechanical properties. Fig. 2b and c show the temperature dependence of  $Q^{-1}$  and  $M'$ , respectively, for a BNBK82 ceramic at different frequencies. In fact, both the  $Q^{-1}$  and  $M'$  curves show strong frequency dependence for temperatures below 450 K

which reinforce the **possible** correlation between dielectric relaxation with a mechanical origin, such as internal stresses, **as observed in other ferroelectric systems were ferroelastic distortions in the paraelectric-ergodic temperature regime are the cause of relaxor state** [58]. For temperatures between 420 and 440 K, the  $Q^{-1}$  curves show peaks and  $M'$  undergoes an abrupt inversion (dip) in the elastic softening tendency. It is well established that these anelastic anomalies are strictly related to structural phase transitions [30,57,59–62]. However, the nature of this transition, and especially the observed frequency-dependence of  $Q^{-1}$  and  $M'$  must be better understood.

On the other hand, the dielectric ( $\epsilon'$ ) peak at  $T_m$  does not have any equivalent mechanical anomaly in the  $Q^{-1}$  and  $M'$  curves. This is one more argument to rule out any possible phase transition at that temperature.

Returning discussion to the temperature region between 420 and 440 K where the phase transition occurs, note that the  $Q^{-1}$  peak and  $M'$  minimum are shifted to higher temperatures as the frequency is increased. This, together with the frequency dispersion are typical characteristics found in materials with strain glass behavior, which occurs when long-range ordering transition is suppressed [12,13,17,19]. The strain glass is the elastic analogous of spin glass in ferromagnets and relaxor in ferroelectrics, being these peculiar characteristics unified under the terminology of ferroic glass [12,13]. Recently, it has been reported that the increase of point defects breaks and gradually suppresses the long-range strain ordering up to a critical concentration where a short-range state, i.e., a strain glass state emerges [12,13,17,19]. Next, the causes that give rise to such dielectric and mechanical behavior in BNBK82 ceramics will be carefully investigated.

Ferroic glass transitions are due the freezing of disordered ferroic states. As for other phenomena of glassy dynamics, the key experimental evidence is the existence of a frequency-dependent susceptibility anomaly at the transition temperature  $T_D$ , usually following a Vogel-Fulcher relation [12]:

$$f(T_D) = f_0 e^{-\frac{E_a}{k_B(T_D - T_0)}} \quad (1)$$

where  $f(T_D)$  represents the frequency of the stimulus,  $f_0$  the frequency pre-exponential factor,  $E_a$  the activation energy,  $k_B$  the Boltzmann constant, and  $T_0$  the freezing temperature. Note that  $T_D$  is the dip temperature from the  $M'$  curves for the case of a strain glass transition. Fig. 3 shows the natural logarithm of the frequency as a

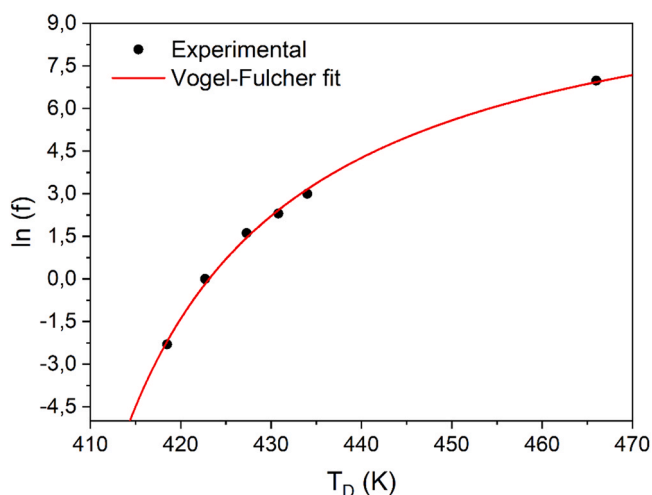


Fig. 3. Natural logarithm of the frequency as a function of  $T_D$  of  $M'$  and its fitting using Eq. (1). for a BNBK82 ceramic.

function of  $T_D$  and its fitting using Eq.1. Experimental data are in very good agreement with the Vogel-Fulcher relation, which is clear evidence of the strain glass character of the phase transition. From the Vogel-Fulcher fitting,  $E_a = (0.029 \pm 0.004)$  eV ( $E_a/k_B = 336$  K) which is very similar to other cases previously reported for strain glass transitions [19] and at least one order of magnitude smaller than those of the typical relaxation processes in BNT-based ceramics [57],  $T_0 = (393.9 \pm 2.5)$  K and  $f_0 = (1.161 \pm 0.003) \times 10^5$  Hz. Note that this transition process thermally activates from 336 K, coinciding very well with the temperature range where  $P_m$  starts to decrease and the peak splitting occurs in the current density loops (see Fig. 1). Also, the freezing temperature is in good agreement with the temperature ( $\sim 400$  K) where  $P_r$  and  $E_c$  remain constant and the hysteresis curves become typical slim loops (see Fig. 1).

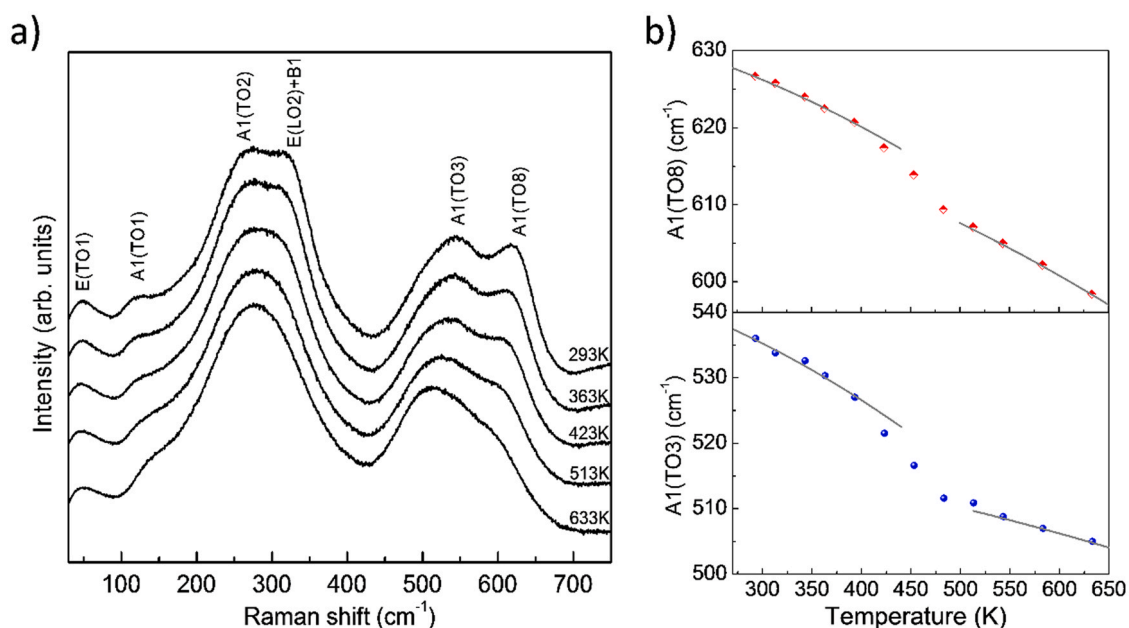
According to previous analyses, the cause of the observed ferroic glass behavior (relaxor and strain glass) must be related to the mixture of polar and non-polar phases and/or to internal stresses caused by point defects, **as already reported for other ferroic materials** [12,51]. The thermal evolution of the crystalline structure was analyzed by Raman spectroscopy and "in situ" high-resolution synchrotron XRD measurements to elucidate the physical origin of this phenomenon in BNBK82 ceramics.

Fig. 4a shows selected Raman spectra of the BNBK measured as a function of temperature. For each temperature, the Raman spectra were reduced by the Bose-Einstein factor  $[1 + 1/(e^{h\nu/k_B T} - 1)]$  to eliminate the temperature-dependent Rayleigh contribution. The spectrum taken at room temperature (on the top) presents a similar profile to that found in BNT-based in tetragonal symmetry, with the most prominent peaks assigned with their corresponding vibrational modes [63–65]. One fingerprint of the  $P4mm$  tetragonal symmetry is the presence of the right-side shoulder in the band  $200\text{--}400\text{ cm}^{-1}$  at around  $320\text{ cm}^{-1}$ , which arises from the contribution of  $E(\text{LO2}) + B1$  modes related to the Ti–O stretching vibrations [64]. When temperature is increased above 400 K the spectral components of this band rearrange, forming a nearly symmetric profile with a well-defined maximum. Such remarkable modification in Raman spectra occurs over a temperature interval similar to that where a peak in  $Q^{-1}$  and a dip in  $M'$  are observed, in addition to being coincident with the calculated freezing temperature  $T_0$ . The band at  $400\text{--}700\text{ cm}^{-1}$ , which is associated with stretching modes related to the  $\text{TiO}_6$  oxygen octahedra [66], is also clearly affected by heating. The splitting of the band in two well-defined peaks  $A1(\text{TO3})$  and  $A1(\text{TO8})$  with similar intensities found in the room temperature spectrum is also a typical signature of the  $P4mm$  symmetry BNT-based systems [67]. The modification in such profile when temperature is increased can be seen as an additional indication of the loss of  $P4mm$  symmetry.

The effects of temperature on the lattice vibrations can be quantitatively evaluated by following the temperature-dependent anharmonicity of the phonons, in which a zone-center optical phonon decays to acoustic ones in a four-phonon process. The relation between the resulting peak wavenumber and the temperature  $\omega(T)$  is given by the monotonic function [68].

$$\omega(T) = \omega_0 + A \left[ 1 + \frac{2}{e^{\frac{h\omega_0}{2k_B T}} - 1} \right] + B \left[ 1 + \frac{3}{e^{\frac{h\omega_0}{3k_B T}} - 1} + \frac{3}{(e^{\frac{h\omega_0}{3k_B T}} - 1)^2} \right] \quad (2)$$

Where  $\omega_0$ ,  $A$  and  $B$  have specific values for each lattice mode.  $k_B$  and  $h$  are, respectively, the Boltzmann and Planck constants. For these analyses we determined the evolution with temperature of the two peaks in the region associated with stretching modes of  $\text{TiO}_6$  oxygen octahedra, by fitting the band at higher wavenumbers. In Fig. 4b is seen that for temperatures up to 400 K, the wavenumbers of both



**Fig. 4.** (a) BNBK82 Raman spectra for selected temperatures, from ambient (top) to 633 K (bottom). (b) Evolution with temperature of the two modes in the higher energy band.

**Table 1**

Anharmonic parameter for the vibrational modes A1(TO3) and A1(TO8) in two temperature ranges.

Mode	Lower temperature			Higher temperature		
	$\omega_0$ (cm <sup>-1</sup> )	A (cm <sup>-1</sup> )	B (cm <sup>-1</sup> )	$\omega_0$ (cm <sup>-1</sup> )	A (cm <sup>-1</sup> )	B (cm <sup>-1</sup> )
A1(TO3)	552.0	-3.3	-2.4	523.7	-2.6	-0.5
A1(TO8)	639.2	-3.2	-2.2	627.5	-2.3	-1.6

modes smoothly decrease, as expected for the temperature-induced softening of the mode. By adjusting Eq. (2) to the experimental data in this temperature range, we calculated the parameters  $\omega_0$ , A and B for each mode. The resulting functions are shown as lines. Remarkably, for temperatures higher than 400 K, the wavenumbers of both modes drastically drop and do not follow the four-phonon process model. Such deviations must be caused only by effects other than the regular heating-related softening and indicate the occurrence of structural modifications. For temperatures higher than 500 K the evolutions of both modes start to follow again the thermal anharmonic shift predicted by Eq. (2). The frequencies in such range, however, clearly present different dependence with temperature  $\omega(T)$ , as evidence that the anharmonicity parameters are different from those calculated for the lower temperatures. The parameters for the two ranges of temperature are shown in Table 1.

The distinct anharmonicities of each mode in the two extreme temperature intervals prove that the Raman signal is predominantly originated in different structures in these two ranges. It is important to consider that no Raman scattering is expected from cubic structures due to their centrosymmetric character. Then, the analysis of data in Fig. 4 are only sensitive to structures with non-centrosymmetric tetragonal symmetry. The identified changes in the fundamental characteristic of the phonons expressed by the parameters in Table 1 indicate the predominant presence of two different types of tetragonal phases in the two temperature extremes intervals. This is especially noticeable through the significant change in  $\omega_0$  value, which represents the natural frequency of the phonons. Since A1(TO3) and A1(TO8) are stretching modes of oxygen octahedra, the

changes in  $\omega_0$  can be interpreted as a renormalization of the phonon eigenvalues due to the octahedral tilt in *P4bm* (existing at higher temperature range), in comparison with *P4mm* structure (at lower temperature regime) where the octahedra are aligned along the *c* direction.

The XRD pattern of a BNBK82 ceramic at room temperature (298 K) can be seen in Fig. 5a. As expected, the peaks were identified as belonging to a perovskite-type structure with *P4mm* symmetry. Identifying the coexistence of *P4mm* and *P4bm* phases in BNT-based ceramics is sometimes very difficult due to the frequent overlapping of the peaks of both phases. Here, the high-resolution synchrotron measurement allowed to resolve the overlap of the peaks around  $2\theta = 46.5^\circ$  as shown in the inset of Fig. 5a. A central asymmetric peak at  $46.55^\circ$  (composed of two peaks) with shoulders on the left ( $46.10^\circ$ ) and the right ( $46.70^\circ$ ) can be clearly observed. The central peaks were identified as belonging to the *P4bm* symmetry, while the shoulders belong to the *P4mm* one. This confirms the coexistence of the *P4mm* and *P4bm* tetragonal phases at room temperature for this BNBK82 ceramic. A rough estimate of the fraction of each phase was made from a Gaussian fit with four peaks for the observed reflection around  $2\theta = 32.4^\circ$ , where the highest peaks of both phases are expected. This can be seen in the inset on the top of Fig. 5a. In this way, the BNBK82 ceramic has an approximate fraction of 75 and 25 wt% of *P4mm* and *P4bm* phases, respectively, at room temperature.

Fig. 5b. shows the temperature evolution from 298 to 773 K of the characteristic diffraction peaks close to  $46.5^\circ$ . The shoulders at  $46.10^\circ$  and  $46.70^\circ$ , which are associated with the (002) and (200) planes of the *P4mm* phase, respectively, have their height starting to decrease slightly above 330 K until around 448 K, where they disappear. For a better view, see the inset on the left of Fig. 5b. Furthermore, between 330 and 373 K, the height of the intermediate peak begins to increase up to 448 K, where it remains approximately constant. This is accompanied by an abrupt shift in the position of the maximum to lower values of  $2\theta$ . The aforementioned features evidence that in the temperature region between 330 and 448 K the *P4mm* phase fraction undergoes a phase transition. The emerging phase was identified from the new  $2\theta$  value of the peak, being the cubic *Pm-3m* phase.

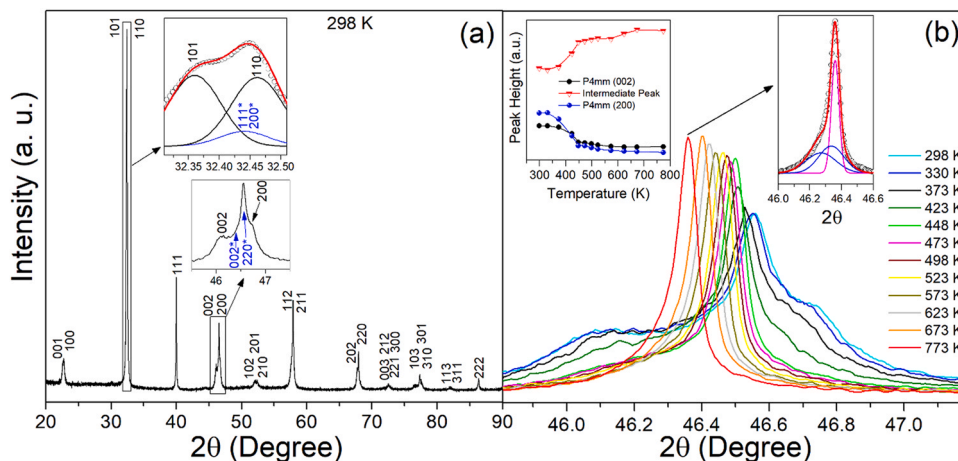


**Fig. 5.** (a) XRD pattern of a BNBK82 ceramic at room temperature (298 K). Insets show magnification of the peaks around  $2\theta = 32.4^\circ$  and  $2\theta = 46.5^\circ$ . Inset on the top also shows a Gaussian fit with four peaks for the observed experimental peak. The hkl planes represented with an asterisk in the insets belong to the  $P4bm$  symmetry. (b) Temperature evolution from 298 to 773 K of the characteristic diffraction peaks close to  $46.5^\circ$ . The inset on the left shows the peak height as a function of temperature for the shoulders at  $46.10^\circ$  and  $46.70^\circ$  and for the intermediate peak. The inset on the right shows the asymmetrical peak at 773 K and its fit using three Gaussian peaks. The peaks were identified from the ICSD cards 230435, 189275 and 280985 belonging to the  $P4mm$ ,  $P4bm$  and  $Pm-3m$  symmetries, respectively.

The small fraction ( $\sim 25\%$ ) of a weakly polar phase ( $P4bm$ ) embedded in a non-polar cubic one is the ideal condition for the long-range polar state breakdown with the consequent formation of a non-ergodic state with  $P4bm$  PNRs. This happens between 400 and 450 K, being the origin of the relaxor behavior and the slim loops, observed in the dielectric and hysteresis measurements, respectively. On the other hand, Ji et al. [19] recently demonstrated a new type of strain glass state in  $\text{LaAlO}_3$  based ceramics, the "tilt" strain glass. In that case, the spontaneous strain arises from the coupling with the tilt of  $\text{AlO}_6$  octahedron, which alternately tilted clockwise and anticlockwise. This is also the case of the  $P4bm$  phase, where the in-phase  $a^0a^0c^+$  oxygen octahedra tilts, which results in the antiparallel ordering of dipole moments [40,41], and in spontaneous strain. In the temperature region where this phase is distributed in nano-regions, a state with short-range ordered strain emerges and a typical strain glass behavior would be expected. Note, from the inset on the left of Fig. 5b, that the height of the intermediate peak remains almost unchanged between 448 and 573 K, while its position shifts linearly to the left, as expected due to thermal expansion. This is an indication that there are no significant structural changes in the material in this temperature range, which is other fingerprint of a tilt strain glass transition, i.e., the invariance of average structure over the whole transition temperature [19].

From 573 to 773 K, the height of the intermediate peak increases again (see inset on the left of Fig. 5b). This can only be related to the increase in the amount of the  $Pm-3m$  cubic phase, which indicates that the  $P4bm$  phase begins to transform into  $Pm-3m$  around 573 K. However, at 773 K, this peak has an asymmetrical appearance with an elongation on the left (see inset on the right of Fig. 5b), which indicates that even at this temperature there is  $P4bm$  phase. Thus, the phase transition from  $P4bm$  to  $Pm-3m$  occurs over a wide temperature region that extends from 573 K to temperatures above 773 K. This is similar to other titanates, especially  $\text{BaTiO}_3$ -based ones, where PNRs are observed up to hundreds of Kelvins above the Curie temperature [69,70].

The physical characterizations performed in this work demonstrated the BNBK82 ceramic is a ferroic glass at temperatures above  $\sim 400$  K, where the relaxor ferroelectric and strain glass characteristics are simultaneously observed. The rigorous analysis of these physical characterizations together with additional structural

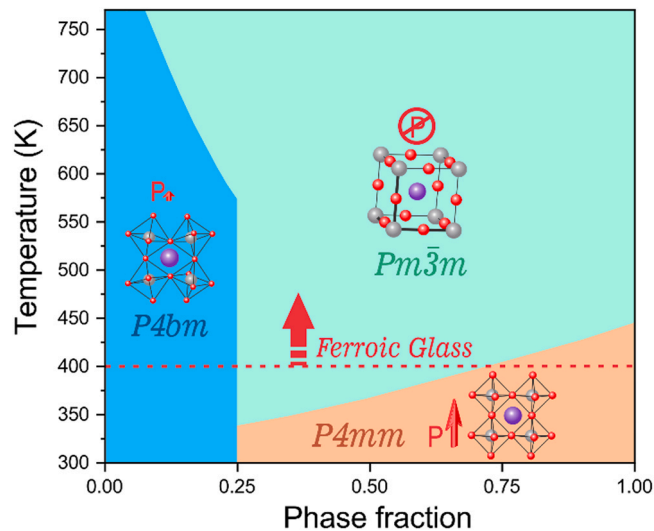


**Fig. 6.** Sketch map illustrating the phase evolution for a BNBK82 material, where the arrow together of the P symbol represents the polarization of each phase.

characterization techniques, such as Raman spectroscopy and XRD, allowed us to clearly elucidate the physical origin of this interesting phenomenon. **To summarize this, the temperature evolution of the structural phases for a BNBK82 material is illustrated in the Fig. 6.**

#### 4. Conclusions

In summary, the hysteresis and current density loops measurements at different temperatures together with the dielectric and anelastic characterizations of BNBK82 ceramics demonstrate the occurrence of a phase transition with relaxor and strain glass characteristics between 400 and 450 K. This simultaneous occurrence of two ferroic glass states opens up broad spectra of possible technological application for this ternary ceramic composition. The origin of this feature was elucidated with the help of Raman spectroscopy and "in situ" high-resolution synchrotron XRD measurements.

Coexistence of the tetragonal  $P4mm$  and  $P4bm$  phases occurs at room temperature with approximate phase fractions of 75 % and 25 %. As the temperature increases, the  $P4mm$  tetragonal phase begins to transform into cubic  $Pm-3m$  near 330 K until about 450 K, where it disappears. From this temperature, the material is composed of  $P4bm$  PNRs embedded in a non-polar cubic matrix, which is the origin of the observed relaxor state. The typical octahedra tilts of the  $P4bm$  PNRs result in spontaneous strain and hence, a tilt strain glass state also arises. Knowing the origin of the phenomenon observed in this BNT-based ternary system, new lead-free ferroic glass materials with improved properties can be designed.

### CRedit authorship contribution statement

**Julio Cesar Camilo Albornoz Diaz:** Investigation, Writing – original draft. **Michel Venet:** Formal analysis, Visualization, Funding acquisition, Resources, Writing – original draft, Writing – review & editing. **Ariano De Giovanni Rodrigues:** Investigation, Formal analysis, Visualization, Writing – original draft. **David Antonio Barbosa Quiroga:** Investigation. **Francesco Cordero:** Investigation, Resources, Formal analysis, Writing – review & editing. **Paulo Sergio da Silva Jr:** Conceptualization, Methodology, Formal analysis, Visualization, Funding acquisition, Resources, Writing – original draft, Writing – review & editing, Supervision.

### Declaration of Competing Interest

The authors declare that they have no known competing financial interests or personal relationships that could have appeared to influence the work reported in this paper.

### Acknowledgments

This work was funded by the São Paulo Research Foundation FAPESP (Grants #2012/08457-7, #2013/00134-7 and #2017/17872-1) and the Coordenação de Aperfeiçoamento de Pessoal de Nível Superior – Brasil (CAPES) – Finance code 001 (Processes 88881.030500/2013-01 and 88881.062225/2014-01). M.V. acknowledges support from Brazilian CNPq (Process 304144/2021-5) This research used facilities of the Brazilian Synchrotron Light Laboratory (LNLS), part of the Brazilian Center for Research in Energy and Materials (CNPem), a private non-profit organization under the supervision of the Brazilian Ministry for Science, Technology, and Innovations (MCTI). The XRD2 beamline staff is acknowledged for the assistance during the experiments of the Proposals nos. 20160310 and 20160688.

### References

- [1] V. Wadhawan, Introduction to Ferroic Materials, CRC Press, 2000, <https://doi.org/10.1201/9781482283051>
- [2] K. Uchino, Ferroelectric Devices, CRC Press, 2018, <https://doi.org/10.1201/b15852>
- [3] J. Puebla, J. Kim, K. Kondou, Y. Otani, Spintronic devices for energy-efficient data storage and energy harvesting, Commun. Mater. 1 (2020) 24, <https://doi.org/10.1038/s43246-020-0022-5>
- [4] E. Salje, Phase transitions in ferroelastic and co-elastic crystals, Ferroelectrics 104 (1990) 111–120, <https://doi.org/10.1080/00150199008223816>
- [5] K. Aizu, Possible species of ferromagnetic, ferroelectric, and ferroelastic crystals, Phys. Rev. B 2 (1970) 754–772, <https://doi.org/10.1103/PhysRevB.2.754>
- [6] B.B. Van Aken, J.-P. Rivera, H. Schmid, M. Fiebig, Observation of ferroelectric domains, Nature 449 (2007) 702–705, <https://doi.org/10.1038/nature06139>
- [7] H. Schmid, Multi-ferroic magnetoelectrics, Ferroelectrics 162 (1994) 317–338, <https://doi.org/10.1080/00150199408245120>
- [8] T. Lottermoser, D. Meier, A short history of multiferroics, Phys. Sci. Rev. 6 (2021), <https://doi.org/10.1515/psr-2020-0032>
- [9] G.A. Smolenskii, A.I. Agranovskaya, Dielectric polarization of a number of complex compounds, Sov. Phys.-Solid State 1 (1960) 1429–1437.
- [10] V. Cannella, J.A. Mydosh, Magnetic ordering in gold-iron alloys, Phys. Rev. B 6 (1972) 4220–4237, <https://doi.org/10.1103/PhysRevB.6.4220>
- [11] S. Sarkar, X. Ren, K. Otsuka, Evidence for strain glass in the ferroelastic-martensitic system  $Ti_{50-x}Ni_{50+x}$ , Phys. Rev. Lett. 95 (2005) 205702, <https://doi.org/10.1103/PhysRevLett.95.205702>
- [12] X. Ren, Strain glass and ferroic glass – unusual properties from glassy nanodomains, Phys. Status Solidi 251 (2014) 1982–1992, <https://doi.org/10.1002/pssb.201451351>
- [13] Y. Ji, D. Wang, Y. Wang, Y. Zhou, D. Xue, K. Otsuka, Y. Wang, X. Ren, Ferroic glasses, Npj Comput. Mater. 3 (2017) 43, <https://doi.org/10.1038/s41524-017-0039-6>
- [14] D. Wang, Z. Zhang, J. Zhang, Y. Zhou, Y. Wang, X. Ding, Y. Wang, X. Ren, Strain glass in Fe-doped Ti–Ni, Acta Mater. 58 (2010) 6206–6215, <https://doi.org/10.1016/j.actamat.2010.07.040>
- [15] Y. Zhou, D. Xue, X. Ding, K. Otsuka, J. Sun, X. Ren, High temperature strain glass transition in defect doped Ti–Pd martensitic alloys, Phys. Status Solidi 251 (2014) 2027–2033, <https://doi.org/10.1002/pssb.201350360>
- [16] Y. Wang, C. Huang, J. Gao, S. Yang, X. Ding, X. Song, X. Ren, Evidence for ferromagnetic strain glass in Ni–Co–Mn–Ga Heusler alloy system, Appl. Phys. Lett. 101 (2012) 101913, <https://doi.org/10.1063/1.4751250>
- [17] Y. Ni, Z. Zhang, D. Wang, Y. Wang, X. Ren, The effect of point defects on ferroelastic phase transition of lanthanum-doped calcium titanate ceramics, J. Alloy. Compd. 577 (2013) S468–S471, <https://doi.org/10.1016/j.jallcom.2012.02.021>
- [18] Y. Yao, Y. Yang, S. Ren, C. Zhou, L. Li, X. Ren, Ferroelastic and strain glass transition in  $(1-x)(Bi_{0.5}Na_{0.5})TiO_{3-x}BaTiO_3$  solid solution, EPL 100 (2012) 17004, <https://doi.org/10.1209/0295-5075/100/17004>
- [19] Y. Ji, P. Zhang, L. He, D. Wang, H. Luo, K. Otsuka, Y. Wang, X. Ren, Tilt strain glass in Sr and Nb co-doped  $LaAlO_3$  ceramics, Acta Mater. 168 (2019) 250–260, <https://doi.org/10.1016/j.actamat.2019.02.007>
- [20] T. Saito, T. Furuta, J.-H. Hwang, S. Kuramoto, K. Nishino, N. Suzuki, R. Chen, A. Yamada, K. Ito, Y. Seno, T. Nonaka, H. Ikehata, N. Nagasako, C. Iwamoto, Y. Ikuhara, T. Sakuma, Multifunctional alloys obtained via a dislocation-free plastic deformation mechanism, Science (80-) 300 (2003) 464–467, <https://doi.org/10.1126/science.1081957>
- [21] Y. Wang, J. Gao, H. Wu, S. Yang, X. Ding, D. Wang, X. Ren, Y. Wang, X. Song, J. Gao, Strain glass transition in a multifunctional  $\beta$ -type Ti alloy, Sci. Rep. 4 (2014) 3995, <https://doi.org/10.1038/srep03995>
- [22] J. Rödel, J.F. Li, Lead-free piezoceramics: status and perspectives, MRS Bull. 43 (2018) 576–580, <https://doi.org/10.1557/mrs.2018.181>
- [23] J. Rödel, W. Jo, K.T.P. Seifert, E.-M. Anton, T. Granzow, D. Damjanovic, Perspective on the development of lead-free piezoceramics, J. Am. Ceram. Soc. 92 (2009) 1153–1177, <https://doi.org/10.1111/j.1551-2916.2009.03061.x>
- [24] T.R. Shrout, S.J. Zhang, Lead-free piezoelectric ceramics: alternatives for PZT? J. Electroceram. 19 (2007) 113–126, <https://doi.org/10.1007/s10832-007-9047-0>
- [25] E. Aksel, J.L. Jones, Advances in lead-free piezoelectric materials for sensors and actuators, Sensors 10 (2010) 1935–1954, <https://doi.org/10.3390/s100301935>
- [26] D. Damjanovic, N. Klein, J. Li, V. Porokhonsky, What can be expected from lead-free piezoelectric materials? Funct. Mater. Lett. 03 (2010) 5–13, <https://doi.org/10.1142/S1793604710000919>
- [27] K. Reichmann, A. Feteira, M. Li, Bismuth sodium titanate based materials for piezoelectric actuators, Materials 8 (2015) 8467–8495, <https://doi.org/10.3390/ma8125469>
- [28] M. Li, M.J. Pietrowski, R.A. De Souza, H. Zhang, I.M. Reaney, S.N. Cook, J.A. Kilner, D.C. Sinclair, A family of oxide ion conductors based on the ferroelectric perovskite  $Na_{0.5}Bi_{0.5}TiO_3$ , Nat. Mater. 13 (2014) 31–35, <https://doi.org/10.1038/nmat3782>
- [29] T. Takenaka, K. Maruyama, K. Sakata,  $(Bi_{1/2}Na_{1/2})TiO_3$ - $BaTiO_3$  system for lead-free piezoelectric ceramics, Jpn. J. Appl. Phys. 30 (1991) 2236–2239, <https://doi.org/10.1143/jjap.30.2236>
- [30] F. Cordero, F. Craciun, F. Trequattrini, E. Mercadelli, C. Galassi, Phase transitions and phase diagram of the ferroelectric perovskite  $(Na_{0.5}Bi_{0.5})_{1-x}Ba_xTiO_3$  by anelastic and dielectric measurements, Phys. Rev. B 81 (2010) 144124, <https://doi.org/10.1103/PhysRevB.81.144124>
- [31] D.A.B. Quiroga, J.C.C. Albornoz Diaz, M. Venet, A.D.G. Rodrigues, O. Florêncio, P.S. da Silva, Evolution of crystalline phases and morphotropic phase boundary of the  $(Bi,Na)TiO_3$ - $(Bi,K)TiO_3$ - $BaTiO_3$  lead-free ceramic system, J. Alloy. Compd. 691 (2017) 498–503, <https://doi.org/10.1016/j.jallcom.2016.08.270>
- [32] Y. Yao, Z. Sun, Y. Ji, Y. Yang, X. Tan, X. Ren, Evolution of the tetragonal to rhombohedral transition in  $(1-x)(Bi_{1/2}Na_{1/2})TiO_{3-x}BaTiO_3$  ( $x \leq 7\%$ ), Sci. Technol. Adv. Mater. 14 (2013) 035008, <https://doi.org/10.1088/1468-6996/14/3/035008>
- [33] J. Glaum, Y. Heo, M. Acosta, P. Sharma, J. Seidel, M. Hinterstein, Revealing the role of local stress on the depolarization of BNT–BT-based relaxors, Phys. Rev. Mater. 3 (2019) 54406, <https://doi.org/10.1103/PhysRevMaterials.3.054406>
- [34] Z. Fan, C.A. Randall, Engineering the nature of polarization dynamics in lead-free relaxors based on  $(Bi_{1/2}Na_{1/2})TiO_3$ , Appl. Phys. Lett. 119 (2021) 112904, <https://doi.org/10.1063/5.0064160>
- [35] J. Kreisel, A.M. Glazer, G. Jones, P.A. Thomas, L. Abello, G. Lucazeau, An x-ray diffraction and Raman spectroscopy investigation of A-site substituted perovskite compounds: the  $(Na_{1-x}K_x)_{0.5}Bi_{0.5}TiO_3$  (Olexle1) solid solution, J. Phys. Condens. Matter 12 (2000) 3267–3280, <https://doi.org/10.1088/0953-8984/12/14/305>
- [36] F. Cordero, L.D. Bella, F. Corvasce, P.M. Latino, A. Morbidini, An insert for anelastic spectroscopy measurements from 80 K to 1100 K, Meas. Sci. Technol. 20 (2008) 15702, <https://doi.org/10.1088/0957-0233/20/1/015702>
- [37] Y. Guo, Y. Liu, R.L. Withers, F. Brink, H. Chen, Large electric field-induced strain and antiferroelectric behavior in  $(1-x)(Na_{0.5}Bi_{0.5})TiO_{3-x}BaTiO_3$  ceramics, Chem. Mater. 23 (2011) 219–228, <https://doi.org/10.1021/cm102719k>

- [38] G. Viola, H. Ning, X. Wei, M. Deluca, A. Adomkevicius, J. Khaliq, M. John Reece, H. Yan, Dielectric relaxation, lattice dynamics and polarization mechanisms in  $\text{Bi}_{0.5}\text{Na}_{0.5}\text{TiO}_3$ -based lead-free ceramics, *J. Appl. Phys.* 114 (2013) 14107, <https://doi.org/10.1063/1.4812383>
- [39] L. Jin, J. Pang, R. Jing, Y. Lan, L. Wang, F. Li, Q. Hu, H. Du, D. Guo, X. Wei, Z. Xu, L. Zhang, G. Liu, Ultra-slim pinched polarization-electric field hysteresis loops and thermally stable electrostrains in lead-free sodium bismuth titanate-based solid solutions, *J. Alloy. Compd.* 788 (2019) 1182–1192, <https://doi.org/10.1016/j.jallcom.2019.02.329>
- [40] G.O. Jones, P.A. Thomas, Investigation of the structure and phase transitions in the novel A-site substituted distorted perovskite compound  $\text{Na}_{0.5}\text{Bi}_{0.5}\text{TiO}_3$ , *Acta Crystallogr. Sect. B Struct. Sci.* 58 (2002) 168–178, <https://doi.org/10.1107/S0108768101020845>
- [41] Y. Kitanaka, M. Ogino, K. Hirano, Y. Noguchi, M. Miyayama, Y. Kagawa, C. Moriyoishi, Y. Kuroiwa, S. Torii, T. Kamiyama, Crystal structural analyses of ferroelectric tetragonal  $(\text{Bi}_{1/2}\text{Na}_{1/2})\text{TiO}_3$ -7% $\text{BaTiO}_3$  powders and single crystals, *Jpn. J. Appl. Phys.* 52 (2013) 09KD01, <https://doi.org/10.7567/jjap.52.09kd01>
- [42] W. Jo, J. Daniels, D. Damjanovic, W. Kleemann, J. Rödel, Two-stage processes of electrically induced-ferroelectric to relaxor transition in  $0.94(\text{Bi}_{1/2}\text{Na}_{1/2})\text{TiO}_3$ -0.06 $\text{BaTiO}_3$ , *Appl. Phys. Lett.* 102 (2013) 192903, <https://doi.org/10.1063/1.4805360>
- [43] V. Dorcet, G. Trolliard, P. Boullay, The structural origin of the antiferroelectric properties and relaxor behavior of  $\text{Na}_{0.5}\text{Bi}_{0.5}\text{TiO}_3$ , *J. Magn. Magn. Mater.* 321 (2009) 1758–1761, <https://doi.org/10.1016/j.jmmm.2009.02.013>
- [44] G. Trolliard, V. Dorcet, Reinvestigation of phase transitions in  $\text{Na}_{0.5}\text{Bi}_{0.5}\text{TiO}_3$  by TEM. Part II: second order orthorhombic to tetragonal phase transition, *Chem. Mater.* 20 (2008) 5074–5082, <https://doi.org/10.1021/cm800464d>
- [45] C. Ma, H. Guo, S.P. Beckman, X. Tan, Creation and destruction of morphotropic phase boundaries through electrical poling: a case study of lead-free  $(\text{Bi}_{1/2}\text{Na}_{1/2})\text{TiO}_3$ - $\text{BaTiO}_3$ , *Phys. Rev. Lett.* 109 (2012) 107602, <https://doi.org/10.1103/PhysRevLett.109.107602>
- [46] G. Liu, J. Dong, L. Zhang, Y. Yan, R. Jing, L. Jin, Phase evolution in  $(1-x)(\text{Na}_{0.5}\text{Bi}_{0.5})\text{TiO}_3$ - $x\text{SrTiO}_3$  solid solutions: a study focusing on dielectric and ferroelectric characteristics, *J. Mater.* 6 (2020) 677–691, <https://doi.org/10.1016/j.jmat.2020.05.005>
- [47] L. Liu, X. Ma, M. Knapp, H. Ehrenberg, B. Peng, L. Fang, M. Hinterstein, Thermal evolution of polar nanoregions identified by the relaxation time of electric modulus in the  $\text{Bi}_{1/2}\text{Na}_{1/2}\text{TiO}_3$  system, *EPL (Europhys. Lett.)* 118 (2017) 47001, <https://doi.org/10.1209/0295-5075/118/47001>
- [48] C. Luo, D. Bansal, J. Li, D. Viehland, B. Winn, Y. Ren, X. Li, H. Luo, O. Delaire, Neutron and x-ray scattering study of phonon dispersion and diffuse scattering in  $(\text{Na,Bi})\text{TiO}_3$ - $\text{BaTiO}_3$  single crystals near the morphotropic phase boundary, *Phys. Rev. B* 96 (2017) 174108, <https://doi.org/10.1103/PhysRevB.96.174108>
- [49] L. Liu, M. Knapp, L.A. Schmitt, H. Ehrenberg, L. Fang, H. Fuess, M. Hoelzel, M. Hinterstein, Structure and dielectric dispersion in cubic-like  $0.5\text{K}_{0.5}\text{Na}_{0.5}\text{NbO}_3$ - $0.5\text{Na}_{1/2}\text{Bi}_{1/2}\text{TiO}_3$  ceramic, *EPL (Europhys. Lett.)* 114 (2016) 47011, <https://doi.org/10.1209/0295-5075/114/47011>
- [50] L. Liu, M. Knapp, H. Ehrenberg, L. Fang, H. Fan, L.A. Schmitt, H. Fuess, M. Hoelzel, H. Dammak, M.P. Thi, M. Hinterstein, Average vs. local structure and composition-property phase diagram of  $\text{K}_{0.5}\text{Na}_{0.5}\text{NbO}_3$ - $\text{Bi}_{1/2}\text{Na}_{1/2}\text{TiO}_3$  system, *J. Eur. Ceram. Soc.* 37 (2017) 1387–1399, <https://doi.org/10.1016/j.jeurceramsoc.2016.11.024>
- [51] L.E. Cross, Relaxor ferroelectrics, *Ferroelectrics* 76 (1987) 241–267, <https://doi.org/10.1080/00150198708016945>
- [52] W. Jo, S. Schaab, E. Sapper, L.A. Schmitt, H.-J. Kleebe, A.J. Bell, J. Rödel, On the phase identity and its thermal evolution of lead free  $(\text{Bi}_{1/2}\text{Na}_{1/2})\text{TiO}_3$ -6 mol%  $\text{BaTiO}_3$ , *J. Appl. Phys.* 110 (2011) 74106, <https://doi.org/10.1063/1.3645054>
- [53] G.O. Jones, J. Kreisel, V. Jennings, M.A. Geday, P.A. Thomas, A.M. Glazer, Investigation of a peculiar relaxor ferroelectric:  $\text{Na}_{0.5}\text{Bi}_{0.5}\text{TiO}_3$ , *Ferroelectrics* 270 (2002) 191–196, <https://doi.org/10.1080/00150190211202>
- [54] E. Dul'kin, J. Suchanicz, A. Kania, M. Roth, Peculiar properties of phase transitions in  $\text{Na}_{0.5}\text{Bi}_{0.5}\text{TiO}_3$ - $\text{BaTiO}_3$  ( $0 < x < 6$ ) lead-free relaxor ferroelectrics seen via acoustic emission, *Mater. Res.* 21 (2018), <https://doi.org/10.1590/1980-5373-mr-2017-0953>
- [55] J. Suchanicz, The effect of A.C. and D.C. electric field on the dielectric properties of  $\text{Na}_{0.5}\text{Bi}_{0.5}\text{TiO}_3$  ceramic, *Condens. Matter Phys.* 2 (1999) 649, <https://doi.org/10.5488/CMP.2.4.649>
- [56] I.P. Aleksandrova, A.A. Sukhovskiy, Y.N. Ivanov, Y.E. Yablonskaya, S.B. Vakhrushev, Local and average structure of relaxor  $\text{Na}_{1/2}\text{Bi}_{1/2}\text{TiO}_3$  from the point of view of NMR, *Ferroelectrics* 378 (2009) 16–22, <https://doi.org/10.1080/00150190902844809>
- [57] J.C.C.A. Diaz, J.C. M'Peko, M. Venet, P.S. da Silva, Unveiling the high-temperature dielectric response of  $\text{Bi}_{0.5}\text{Na}_{0.5}\text{TiO}_3$ , *Sci. Rep.* 10 (2020), <https://doi.org/10.1038/s41598-020-75859-z>
- [58] G. Das Adhikary, B. Mahale, A. Senyshyn, R. Ranjan, Relaxor ground state forced by ferroelastic instability in  $\text{K}_{0.5}\text{Bi}_{0.5}\text{TiO}_3$ - $\text{Na}_{0.5}\text{Bi}_{0.5}\text{TiO}_3$ , *Phys. Rev. B* 102 (2020) 184113, <https://doi.org/10.1103/PhysRevB.102.184113>
- [59] P.S. Silva, J.C.C.A. Diaz, O. Florêncio, M. Venet, J.C. M'Peko, Analysis of the phase transitions in BNT-BT lead-free ceramics around morphotropic phase boundary by mechanical and dielectric spectroscopies, *Arch. Metall. Mater.* 61 (2016) 17–20, <https://doi.org/10.1515/amm-2016-0008>
- [60] R. Schaller, G. Fantozzi, G.M. Gremaut, *Mechanical Spectroscopy Q-1 2001: with Applications to Materials Science*, Trans Tech Publications Ltd., Uetikon-Zuerich, CH; Enfield, NH, 2001.
- [61] P.S. Da Silva, M. Venet, O. Florêncio, Influence of diffuse phase transition on the anelastic behavior of Nb-doped  $\text{Pb}(\text{Zr}_{0.53}\text{Ti}_{0.47})\text{O}_3$  ceramics, *J. Alloy. Compd.* 647 (2015) 784–789, <https://doi.org/10.1016/j.jallcom.2015.05.225>
- [62] J.C.C.A. Diaz, M. Venet, F. Cordero, P.S. da Silva, Anelastic and optical properties of  $\text{Bi}_{0.5}\text{Na}_{0.5}\text{TiO}_3$  and  $(\text{Bi}_{0.5}\text{Na}_{0.5})_{0.94}\text{Ba}_{0.06}\text{TiO}_3$  lead-free ceramic systems doped with donor  $\text{Sm}^{3+}$ , *J. Alloy. Compd.* 746 (2018) 648–652, <https://doi.org/10.1016/j.jallcom.2018.02.303>
- [63] J. Anthoniappen, C.S. Tu, P.-Y. Chen, C.-S. Chen, Y.U. Idzerda, S.-J. Chiu, Raman spectra and structural stability in B-site manganese doped  $(\text{Bi}_{0.5}\text{Na}_{0.5})_{0.925}\text{Ba}_{0.075}\text{TiO}_3$  relaxor ferroelectric ceramics, *J. Eur. Ceram. Soc.* 35 (2015) 3495–3506, <https://doi.org/10.1016/j.jeurceramsoc.2015.05.002>
- [64] V. Pal, O.P. Thakur, R.K. Dwivedi, Investigation of MPB region in lead free BLNT-BCT system through XRD and Raman spectroscopy, *J. Phys. D Appl. Phys.* 48 (2015) 55301, <https://doi.org/10.1088/0022-3727/48/5/055301>
- [65] P.-Y. Chen, C.-S. Chen, C.-S. Tu, P.-H. Chen, J. Anthoniappen, Effects of texture on microstructure, Raman vibration, and ferroelectric properties in  $92.5\%(\text{Bi}_{0.5}\text{Na}_{0.5})\text{TiO}_3$ - $7.5\%\text{BaTiO}_3$  ceramics, *J. Eur. Ceram. Soc.* 36 (2016) 1613–1622, <https://doi.org/10.1016/j.jeurceramsoc.2016.01.038>
- [66] J. Shi, H. Fan, X. Liu, A.J. Bell, Large electrostrictive strain in  $(\text{Bi}_{0.5}\text{Na}_{0.5})\text{TiO}_3$ - $\text{BaTiO}_3$ - $(\text{Sr}_{0.7}\text{Bi}_{0.2})\text{TiO}_3$  solid solutions, *J. Am. Ceram. Soc.* 97 (2014) 848–853, <https://doi.org/10.1111/jace.12712>
- [67] Y. Mendez-González, A. Peláiz-Barranco, A.L. Curcio, A.D. Rodrigues, J.D.S. Guerra, Raman spectroscopy study of the La-modified  $(\text{Bi}_{0.5}\text{Na}_{0.5})_{0.92}\text{Ba}_{0.08}\text{TiO}_3$  lead-free ceramic system, *J. Raman Spectrosc.* 50 (2019) jrs.5603, <https://doi.org/10.1002/jrs.5603>
- [68] M. Balkanski, R.F. Wallis, E. Haro, Anharmonic effects in light scattering due to optical phonons in silicon, *Phys. Rev. B* 28 (1983) 1928–1934, <https://doi.org/10.1103/PhysRevB.28.1928>
- [69] F. Cordero, F. Trequattrini, D.A.B. Quiroga, P.S. Silva, Hopping and clustering of oxygen vacancies in  $\text{BaTiO}_3$ - and the influence of the off-centred Ti atoms, *J. Alloy. Compd.* 874 (2021) 159753, <https://doi.org/10.1016/j.jallcom.2021.159753>
- [70] A. Bencan, E. Oveisi, S. Hashemizadeh, V.K. Veerapandiyam, T. Hoshina, T. Rojac, M. Deluca, G. Drazic, D. Damjanovic, Atomic scale symmetry and polar nanoclusters in the paraelectric phase of ferroelectric materials, *Nat. Commun.* 12 (2021) 3509, <https://doi.org/10.1038/s41467-021-23600-3>